Integrated nonlinear Mach Zehnder for 40 Gbit/s all-optical switching

C. Lacava,[1,*] M. J. Strain,[2] P. Minzioni,[1] I. Cristiani,[1] and M. Sorel[2]

[1]*Quantum electronics lab, Department of Electrical, Computer and Biomedical Engineering, University of Pavia, Via Ferrata 5A, IT-27100 Pavia, Italy*
[2]*School of Engineering, University of Glasgow, UK G12 8LT Glasgow, United Kingdom*
[*]*cosimo.lacava01@ateneopv.it*

Abstract: We report on the experimental demonstration of a novel silicon based fully integrated nonlinear Mach Zehnder device. A standard silicon waveguide is used as a nonlinear arm, conversely a large mode SU-8 waveguide acts as a purely linear arm. Given this asymmetry, an intensity dependent phase shift can be introduced between the two interferometric arms. Thanks to a fine tuning of the silicon arm optical properties, a low power, ultrafast, picosecond operation is demonstrated, allowing the use of this device for ultrafast all-optical signal processing in high density communication networks.

OCIS codes: (130.4815) Optical switching devices; (190.4360) Nonlinear optics, devices.

References and links

1. M. Dinu, F. Quochi, and H. Garcia, "Third-order nonlinearities in silicon at telecom wavelengths," Appl. Phys. Lett. **82**(18), 2954–2956 (2003).
2. V. R. Almeida, C. A. Barrios, R. R. Panepucci, and M. Lipson, "All-optical control of light on a silicon chip," Nature **431**(7012), 1081–1084 (2004).
3. H. Rong, Y. H. Kuo, A. Liu, M. Paniccia, and O. Cohen, "High efficiency wavelength conversion of 10 Gb/s data in silicon waveguides," Opt. Express **14**(3), 1182–1188 (2006).
4. F. Morichetti, A. Canciamilla, C. Ferrari, A. Samarelli, M. Sorel, and A. Melloni, "Travelling-wave resonant four-wave mixing breaks the limits of cavity-enhanced all-optical wavelength conversion," Nat Commun **2**, 296 (2011).
5. L. R. Nunes, T. K. Liang, H. K. Tsang, M. Tsuchiya, D. Van Thourhout, P. Dumon, and R. Baets, "Ultrafast non-inverting wavelength conversion by cross-absorption modulation in silicon wire waveguides," *in Proceeding of IEEE Conference on Group IV Photonics* (Institute of Electrical and Electronic Engineers New York, 2005), pp. 154–156.
6. W. Astar, J. B. Driscoll, X. P. Liu, J. I. Dadap, W. M. J. Green, Y. A. Vlasov, G. M. Carter, and R. M. Osgood, "All-optical format conversion of NRZ-OOK to RZ-OOK in a silicon nanowire utilizing either XPM or FWM and resulting in a receiver sensitivity gain of 2.5 dB," IEEE J. Sel. Top. Quantum Electron. **16**(1), 234–249 (2010).
7. D. Cotter, R. J. Manning, K. J. Blow, A. D. Ellis, A. E. Kelly, D. Nesset, I. D. Phillips, A. J. Poustie, and D. C. Rogers, "Nonlinear optics for high- speed digital information processing," Science **286**(5444), 1523–1528 (1999).
8. J. P. Sokoloff, P. R. Prucnal, I. Glesk, and M. Kane, "A terahertz optical asymmetric demultiplexer (TOAD)," IEEE Photon. Technol. Lett. **5**(7), 787–790 (1993).
9. K. J. Blow, N. J. Doran, and B. P. Nelson, "Demonstration of the nonlinear fibre loop mirror as an ultrafast all-optical demultiplexer," IEEE Electron. Lett. **26**(14), 962–964 (1990).
10. I. Glesk, P. J. Bock, P. Cheben, J. H. Schmid, J. Lapointe, and S. Janz, "All-optical switching using nonlinear subwavelength mach-zehnder on silicon," Opt. Express **19**(15), 14031–14039 (2011).
11. I. Glesk, P. J. Bock, P. Cheben, J. H. Schmid, J. Lapointe, and S. Janz, "Picosecond all-optical switching using nonlinear Mach-Zehnder with silicon subwavelength grating and photonic wire arms," Opt. Quantum Electron. **44**(12-13), 613–621 (2012).
12. T. Shoji, T. Tsuchizawa, T. Watanabe, K. Yamada, and H. Morita, "Low loss mode size converter from 0.3 μm square Si wire waveguides to single mode fibres," IEEE Electron. Lett. **38**(25), 1669–1670 (2002).
13. Q. Lin, O. J. Painter, and G. P. Agrawal, "Nonlinear optical phenomena in silicon waveguides: modeling and applications," Opt. Express **15**(25), 16604–16644 (2007).
14. I. D. Rukhlenko, M. Premaratne, and G. P. Agrawal, "Nonlinear silicon photonics: analytical tools," IEEE J. Sel. Top. Quantum Electron. **16**(1), 200–215 (2010).

15. C. Dorrer and D. N. Maywar, "RF spectrum analysis of optical signals using nonlinear optics," J. Lightwave Technol. **22**(1), 266–274 (2004).
16. L. Shen, N. Healy, P. Mehta, T. D. Day, J. R. Sparks, J. V. Badding, and A. C. Peacock, "Nonlinear transmission properties of hydrogenated amorphous silicon core fibers towards the mid-infrared regime," Opt. Express **21**(11), 13075–13083 (2013).
17. B. Kuyken, H. Ji, S. Clemmen, S. K. Selvaraja, H. Hu, M. Pu, M. Galili, P. Jeppesen, G. Morthier, S. Massar, L. K. Oxenløwe, G. Roelkens, and R. Baets, "Nonlinear properties of and nonlinear processing in hydrogenated amorphous silicon waveguides," Opt. Express **19**(26), B146–B153 (2011).

1. Introduction

Silicon photonics is a well-established platform for the development of fully integrated devices for optical communications system. The high index difference achievable in the SOI (silicon-on-insulator) platform allows the realization of miniaturized waveguide structures (typical width 500 nm) with high beam confinement and very low curvature losses. Due to the reduced mode area and to the strong nonlinear refractive index of bulk silicon [1], ultra high nonlinear effects can be easily achieved in these structures using power levels usually adopted in telecommunication systems. Future high capacity networks will require high speed devices that can perform all-optical signal processing functionalities. Indeed in the last decade many authors have reported on nonlinear devices for optical communication systems based on nonlinear effects in silicon such as all-optical modulators [2], wavelength converters [3,4], optical switching [5], format converters [6], etc.

Integrated semiconductor-based interferometric schemes have been widely adopted for this purpose. The basic idea is to selectively change the optical length of one arm of an interferometer, by using a nonlinear element (NLE), so that the interference condition can be changed by means of an optical control signal. Usually a low power probe signal propagates into the interferometer in the linear regime and a high power control beam is used to trigger the nonlinear regime enabling partial or total switching of the probe from one output port to the other. This technique allows the demonstration of a number of signal processing functionalities, such as wavelength conversion, time-division demultiplexing and switching, intensity modulation and logic gates operations [7,8].

In these devices the NLE is typically a semiconductor optical amplifier (SOA), which is placed asymmetrically with respect to the center of the interferometer loop, and a dedicated port is used to inject the control beam and tuning of the optical propagation regime through the SOA. Two aspects determine the maximum operation speed of these devices: i) the time required to achieve the desired differential phase shift (π in the case of total beam-switching), ii) the time required to recover the initial optical conditions. The onset time can generally be very fast (<1 ps) but typically gain-recovery is hundreds of times longer, thus limiting the maximum operating frequency. Also second order and third order nonlinearities in dielectric materials were exploited in similar schemes to perform all-optical signal processing [9]. In such cases purely electronic nonlinearities are triggered enabling very high speed response. Nevertheless they are usually based on fibers or nonlinear crystals which do not lend themselves to integration in optical micro-circuits.

Here we propose a fully integrated, silicon photonic, all-optical device allowing ultra-fast switching of an optical signal between the two output ports of a Mach Zehnder interferometer (MZI). In this device the NLE is the Si waveguide constituting one arm of the MZI, allowing efficient nonlinear interaction in a short length and low power operation [2]. The other arm of the MZI is a large-area waveguide, made using a SU-8 polymer in which the light intensity is quite low and the nonlinearities can be neglected. This approach is quite different from those proposed in the literature, as the switching is not obtained by selectively coupling a pump in one arm of the interferometer, but by exploiting two arms with strongly different and finely tuned nonlinear properties. In this case the control signal is injected through the MZI input ports, avoiding the need for a dedicated control signal port and consequently reducing the packaging complexity. We note that a similar MZI device based on Si was already proposed

to perform nonlinear optical switching [10,11]. Nevertheless such a device does not rely on standard CMOS compatible fabrication technology and requires demanding lithographic processing in order to write the sub-wavelength grating patterns. In addition a very high optical power (>30 W, peak power) is required and, as a consequence, only low-speed operation was achieved due to the Free Carrier Effect (FCE).

The device reported here is designed to operate with optical powers as low as 600 mW and therefore does not suffer from two-photon absorption (TPA) and free carrier absorption (FCA). The proposed device exhibits ultrafast operation (>40 Gbit/s) and as such represents a promising building block to achieve all-optical functionalities such as ultrafast demultiplexing, all-optical switching, intensity modulation and logic gates.

In section 2 of the paper we describe the design and fabrication process, and we review the principle of operation of the device. In section 3 we summarize the numerical simulations that we carried out to design the final device and, finally, in section 4 we report on the experimental characterization of the fabricated device.

2. Device scheme and working principle

A schematic representation of inhomogeneous MZI structure is reported in Fig. 1. The two input ports are connected to the two MZI arms by a 4-port 50:50 waveguide coupler/splitter.
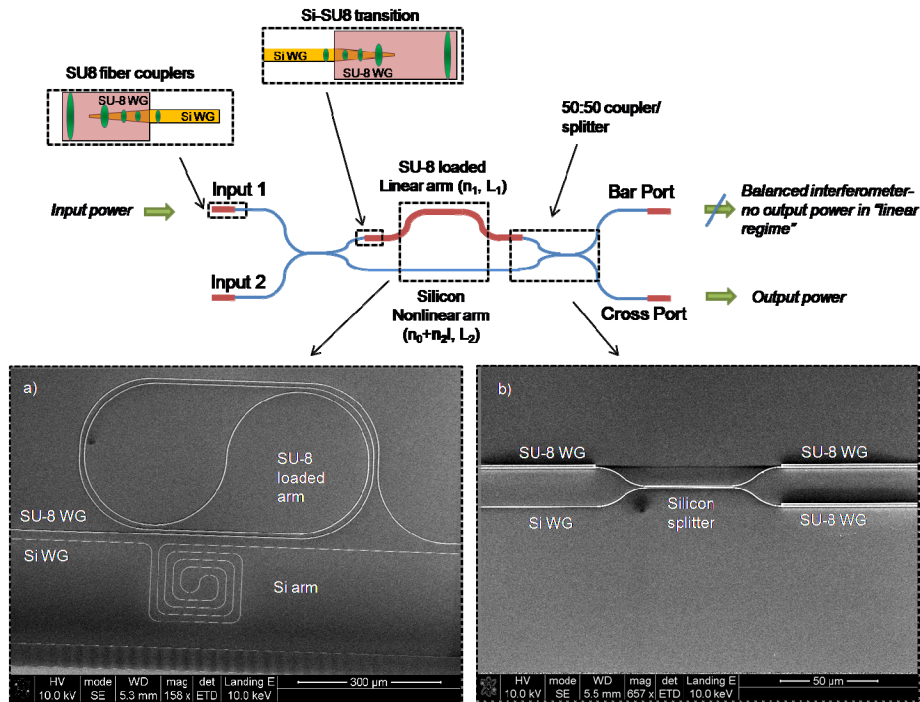

Fig. 1. Schematic of the device. SU8-Silicon (and vice versa) transition are made by means of inverse taper sections (depicted on the top part of the schematic). The lengths of the two arms are designed so that the optical paths, when a low power signal is injected, are equals, and the MZI is balanced. Two SEM images are shown on the bottom: a) two arms of the MZI, on the top the SU8 loaded arm and on the bottom the nonlinear Si arm; b) 50:50 splitter made in silicon.

One arm, constituting the NLE, is a 7.874 mm long silicon strip waveguide realized as a spiral with a cross section of 500x220 nm; conversely the other arm is a SU-8 polymer waveguide with large cross section (the cross section is 2x2 μm so that the optical mode is 15 times larger with respect to the nonlinear arm), with a length L = 12.437 mm. The SU8-waveguide is significantly longer than the Si waveguide to compensate for the effective

refractive index mismatch between the two arms ($n_{eff,Si\ WG}$ = 2.47; $n_{eff,SU8\ WG}$ = 1.57), thus yielding a balanced MZI in the linear regime. As reported in Fig. 1, all of the transitions between Si waveguides and SU-8 waveguides are realized by integrated inverse tapers [12], which are also used for the fiber-to-chip and chip-to-fiber coupling sections. The tapers are 300 μm long (see Fig. 2), and the taper loss has been experimentally evaluated at 0.25 dB/taper by means of dedicated test devices. The small index difference between silica fibers and SU-8 waveguide allows good coupling efficiency (coupling loss < 2 dB by using a small tip lensed fiber).

The device was fabricated on a CMOS-compatible SOI wafer in the James Watt Nanofabrication Center at Glasgow University. Electron beam lithography was used to define the waveguide layout in high contrast hydrogen silsesquioxane (HSQ) resist. After this step, an inductively coupled plasma reactive ion etching (ICP-RIE) was used to transfer the pattern onto the silicon wafer, and the SU-8 waveguide pattern were then defined by using direct e-beam lithography and development. The sample was finally coated by a 2 µm thick Poly (Methyl Methacrylate) PMMA protective layer. Straight waveguides were also fabricated on the same chip to test linear and nonlinear characteristics of the silicon waveguide.
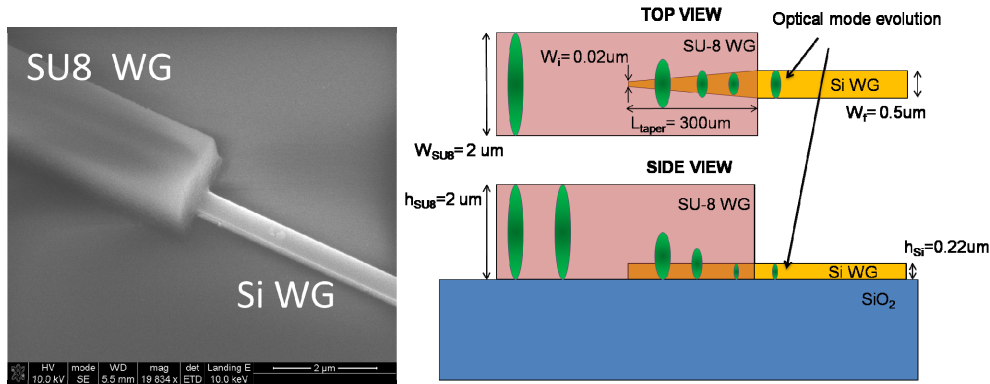

Fig. 2. Inverse taper section scheme used in the final device. On the right hand part a SEM image of the taper is shown.

In a balanced MZI operating in the linear regime all of the optical radiation coupled into the INPUT 1 port is output from the cross-port of the device. In order to change the optical power splitting ratio between the two output ports, a differential phase shift (Δφ) between the two MZI arms is needed. If Δφ = π, all the optical radiation input at the INPUT 1 port is output from the bar-port of the device.

If the differential phase shift can be rapidly increased and decreased, it is possible to change the ratio between the optical power at the two output ports at a high rate, thus allowing the switching of the probe beam (e.g.: from the cross-port to the bar-port) in a selected time-window.

3. Nonlinear effects in silicon and numerical simulations

Our goal is to use the Si arm as a phase shifter by exploiting self- phase modulation (SPM) and cross-phase modulation (XPM), but several nonlinear effects become significant when high optical intensities propagate in a Si waveguide. A detailed analysis of nonlinear effects in Si is needed in order to understand the overall performance of the final device and find the optimal operation regime. In particular, TPA, FCA and free carrier dispersion (FCD) must be included in the analysis to properly evaluate the device performance as their effect can become dominant when the optical intensity into the waveguide is too high, and thus they play a relevant role in determining the optimum interaction length and operating power. We modeled our system by using two coupled Schrodinger equations as follows [13,14]:

$$\frac{\partial A_c}{\partial z} + \frac{\alpha_{lin}}{2} A_c + i\frac{1}{2}\beta_{2c}\frac{\partial^2 A_c}{\partial t^2}$$

$$= i(\gamma |A_c|^2 + 2\gamma |A_p|^2)A_c - \frac{1}{2A_{eff}}(\beta_{TPA}|A_c|^2 + 2\beta_{TPA}|A_p|^2)A_c + \qquad (1.1)$$

$$-N_g\frac{\sigma_c}{2}A_c - iN_g\frac{2\pi k_c}{\lambda_c}A_c.$$

$$\frac{\partial A_p}{\partial z} + \frac{\alpha_{lin}}{2} A_p + i\frac{1}{2}\beta_{2p}\frac{\partial^2 A_p}{\partial t^2}$$

$$= i(\gamma |A_p|^2 + 2\gamma |A_c|^2)A_p - \frac{1}{2A_{eff}}(\beta_{TPA}|A_p|^2 + 2\beta_{TPA}|A_c|^2)A_p + \qquad (1.2)$$

$$-N_g\frac{\sigma_p}{2}A_p - iN_g\frac{2\pi k_p}{\lambda_p}A_p.$$

where $A_{c,p}$ is the slowly varying amplitude of the pulse envelope of the pulsed control signal c and the cw probe p, α is the linear loss coefficient, $\beta_{2c,p}$ are second–order dispersion parameters. The nonlinear coefficient γ is defined as $\gamma = (2\pi n_2)/(\lambda A_{eff})$, where A_{eff} is the silicon waveguide effective area defined in [12], while β_{TPA} is the silicon TPA coefficient [1]. The FCA coefficients σ_c and σ_p are defined as $\sigma_{c,p} = \sigma(\lambda_{c,p}/\lambda_r)^2$, where $\lambda_r = 1550$ nm is the reference wavelength [13]. Finally, $k_{c,p}$ is the FCD coefficient and N_g is the free carrier density generated thought TPA process. N_g can be calculated by using Eq. (1.3) [13–15],where τ_c is the free carrier lifetime which was already measured in silicon [2] and is equal to 1 ns, in the worst case, for our waveguide geometry.

$$\frac{\partial N_g}{\partial t} = \frac{\beta_{TPA}}{2h\nu_c}|A_c|^4 - \frac{N_g}{\tau_g}. \qquad (1.3)$$

From these three equations, one can observe that TPA and FCA strongly influence the loss of cw signals through Cross Absorption Modulation (XAM) as well [13]. For this reason, the optimal power of the control signal has to be determined as a tradeoff between a large switching efficiency and the amount of induced nonlinear loss. The silicon arm acts as a phase shifter that, in the MZI configuration, switches the power from one arm to the other. On the other hand, XAM introduces a nonlinear loss, which contributes to the formation of a "dark pulse" at both the cross and bar output of the MZI. The effects of XAM can be limited by choosing a control-signal power below the level at which the effect of TPA cannot be considered as negligible.

In order to take into account all effects and calculate the TPA and FCA threshold we numerically simulated Eqs. 1.2, 1.3 and 1.4 by means of the split step method [13]. The main waveguide and material parameters used in the simulations are obtained by measuring test waveguides and are reported in Table 1.

Table 1. Waveguide linear and nonlinear parameters used as input in our numerical simulations.

Parameter	Value	Unit
$\sigma_{p,s}$	1.45×10^{-21}	m^2
k_c	1.35×10^{-27}	m^3
β_{TPA}	5×10^{-12}	m/W
n_2	6×10^{-18}	m^2/W
L	7.87	mm
γ	320	(Wm)$^{-1}$
α_{lin}	2.4	dB/cm
A_{eff}	0.1	μm^2

The simulation results, reported in Fig. 3, show the phase-change due to XPM and FCD as a function of the control signal power. If the nonlinear losses are neglected (red line), no phase-change saturation is observed, and the Kerr-induced phase-change is simply given by [13]:

$$\Delta\phi = 2\gamma L_{eff} P_{peak} \qquad (1.4)$$

where $L_{eff} = 1\text{-}exp(\alpha_{lin}L)/\alpha$.

Conversely, a saturation effect is present when TPA, FCA and FCD are taken into account in the simulation, as the power-dependent losses introduced by TPA and FCA reduce the nonlinear interaction length, and FCD introduces a phase-term of opposite sign to that of SPM and XPM. The saturation point is reached when the input power is P_{in} = 29 dBm and the resulting maximum phase shift is equal to $\Delta\phi$ = 82° which corresponds to a maximum switching level of 46%. We note that similar results, in terms of nonlinear phase shift, could be obtained with competing technologies such as highly nonlinear fibers [16]. However a considerably higher nonlinear interaction length must be used to obtain a similar performance and these devices are incompatible with multi-element optical circuit integration. In order to reduce the impact of nonlinear losses, we decided to operate our device with peak pump level values from 20 dBm to 27 dBm.
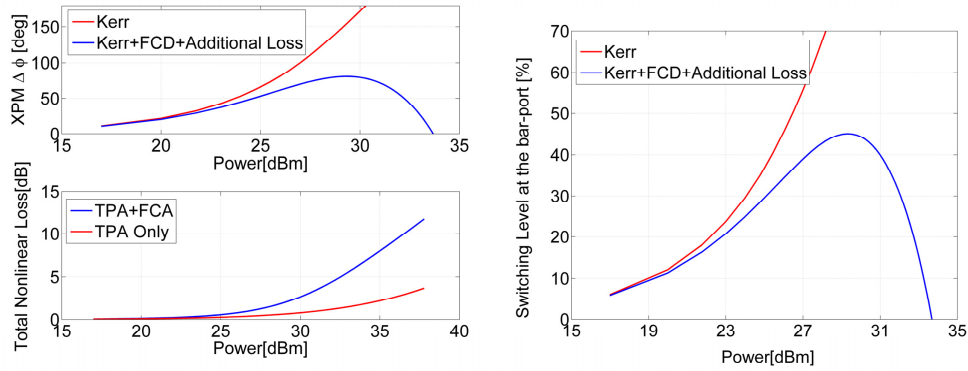

Fig. 3. Split step simulation results for an L = 7.8 mm silicon waveguide. Note that the red lines in the top and right hand panel are exponential curves because the horizontal axis is in dBm units.

4. Nonlinear MZI ultrafast experimental characterization

In order to check the ultrafast signal processing capabilities of the device we first verified that the MZI is perfectly balanced in the whole 1500–1620 nm band; then we performed a set of pump-probe experiments, to calibrate the MZI operation.

The control signal was a pulse train (λ = 1550 nm) generated by a fiber mode-locked laser (Pritel 1550 nm Ultrafast Optical Clock). The pulses, with 10 GHz repetition rate and a pulse width of 2 ps, were first input to a fiber interleaver to obtain a 40 GHz control signal, and then amplified with a high power EDFA (30 dBm IPG photonics-EAD-1K-C).
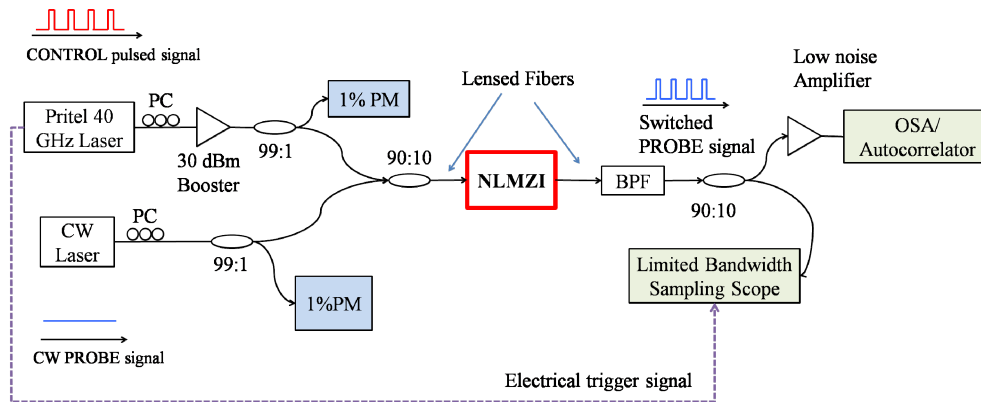
Fig. 4. Nonlinear Mach Zehnder operation set-up scheme. The output band-pass filter (BPF) stage is realized by cascading two slightly different optical filters.

The weak probe signal was emitted by a tunable external cavity laser (Mod. Agilent 8194A). The wavelength was set at $\lambda_s = 1535$ nm, in order to guarantee a high suppression of the pump at the device output by using standard optical filters. Both the clock pump and probe signal powers were monitored through power meters by extracting 1% power by means of tap-couplers (Fig. 4). The control and probe signals were combined by means of a 90/10 coupler to reduce loss on the control beam and launched into the nonlinear MZI by using tapered fibers. The large fiber spot (5 µm) did not match the input taper mode size resulting in additional coupling loss ($\alpha_{coupling} = 9.81$ dB/taper), which were measured by using proper test devices and taken into account in the experimental data analysis.

Both bar- and cross-port output signals were collected at the MZI outputs. The control signal was then filtered out with an optical band-pass filter to ensure a pump suppression of 30 dB with respect to the probe signal, while the probe beam was first sent to a low noise preamplifier, and then to a fast oscilloscope (Agilent Infinium DCA-J 86100C Digital Communication Analyzer).

The device behavior was tested both at 10 Gbit/s and 40 Gbit/s, i.e. without or with the optical interleaver. The oscilloscope traces obtained at 10 Gbit/s with a peak power of the control beam P = 27 dBm (at the input of the MZ silicon arm) are reported in Fig. 5(a). All the data are normalized to the probe signal power level, measured at the cross-port, in the absence of the control signal pulse. The blue trace is the output at the cross-port, while the red trace was measured at the bar-port output. It can be observed that XAM decreases the intensity of the probe signal measured at both the bar- and the cross-port, which, according to the numerical analysis in the purely Kerr regime case (Fig. 3, red line), should be 55% at the bar- port and 45% at the cross-port. As a consequence, the maximum switching level is decreased at the bar-port and a 40% switching ratio was measured for a $P_c = 27$ dBm. This value is in good agreement with the full-numerical analysis (when TPA and FC are taken into account, Fig. 3, blue curves), thus confirming the validity of our numerical model.
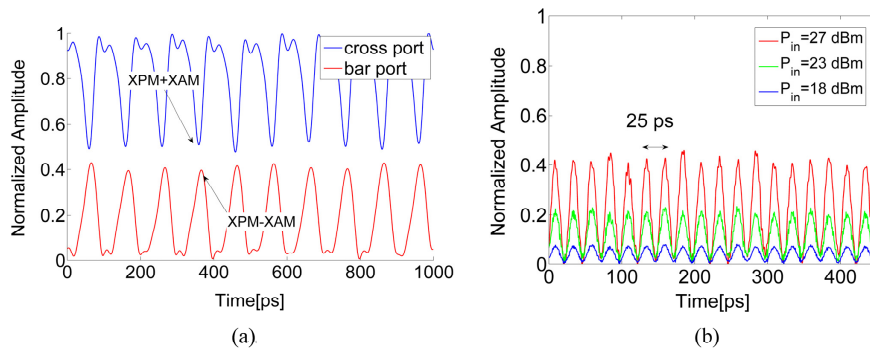
(a)   (b)

Fig. 5. (a) Switching traces at 10 GHz operation for a Pc = 27 dBm (b) Switching traces at 40
GHz operation taken from the bar-port for three different clock peak pump levels

Figure 5(b) shows the switching traces at the bar-port obtained using a control signal with repetition frequency of 40 GHz and for three different peak power levels, 18, 23 and 27 dBm, coupled into the Si waveguide. The normalized amplitude of the probe signal measured at the bar-port is equal to the 7%, 20% and 40% of the probe beam, in good agreement with numerical simulations. Finally, we tested the device by using control signal power levels which were above the TPA theoretical limit of P_c = 27 dBm. Figure 6 shows results for two different control signal peak power levels: the blue line was obtained by using a power level, which is 4 dB higher than the predicted limits. It is clear that TPA and FCA effects strongly affect device operation by reducing the switching ratio to a value of 16%. TPA and FCA become even more dominant if the power is further increased, as confirmed by the 2% switching ratio level that was achieved by using a control signal peak power level of 34 dBm. These results show that experimental investigation is in a good agreement with our numerical simulation, confirming the validity of our design.
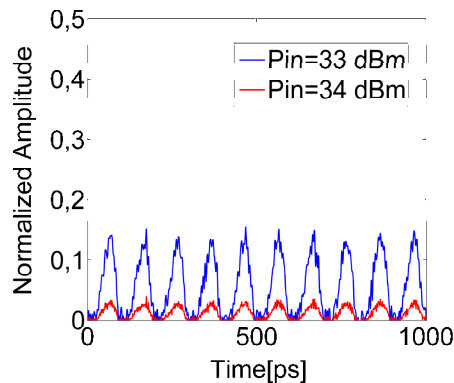

Fig. 6. 10 Gb/s traces taken from the bar-port at control signal peak power which were above
the TPA/FCA limit identified by the numerical simulations. Two traces are shown: the blue
trace corresponds to a control signal peak power of 33 dBm and the red trace to a P_c = 34 dBm.

Finally, in order to evaluate the temporal width of the switching window, different autocorrelation traces at P_c = 18, 23 and 27 dBm of the probe beam were taken. Figure 7 shows the trace corresponding to the maximum power operation, P_c = 27 dBm. The temporal width (FWHM) of the autocorrelation trace is 2 ps, matching that of the input pulse, thus confirming the ultrafast response of this device, where the maximum operating speed is determined by the temporal width of the control signal. The temporal shape of the probe

signal is determined by the combination: of the nonlinear response of the Si arm, and of the nonlinear transfer function of the MZI. As a consequence low level signals (such as noise or other degradation effects) are not transferred at the probe signal wavelength. Hence this device acts also as a pulse re-shaper, which preserves the control signal pulse temporal profile. As a final remark, we note that the output pulse shape (Fig. 7) is in good agreement with the Pritel laser input shape.
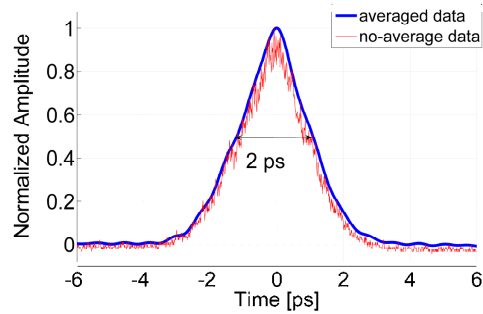

Fig. 7. Autocorrelation trace taken from the bar- port at P_c = 27 dBm. No degradation effects were observed at this pump level and at lower pump levels

5. Conclusion

A novel integrated inhomogeneous nonlinear MZI, silicon based device has been proposed as a basic building block for all-optical signal processing circuits. The proposed device is able to change the output state of an input signal by tuning the optical properties of one arm of the MZI. The use of Si and SU-8 waveguides combined with the strong silicon nonlinearities, allow a co-propagating optical control signal, which can be injected into the device through the same input port as the probe signal. No additional coupler and port are needed and, a 4 port simple structure can be used. Device response time is lower than 2 ps making it very promising as an ultrafast de-multiplexer for high density optical communication networks. Low power operation was also demonstrated, achieving a power unbalancing between the output ports of 40% by using a control pump peak level of 27 dBm, which is 10 dB less than that used in a similar device [10,11]. No signal degradation is observed at pump levels below the TPA/FCA power threshold predicted by numerical simulations. As a final remark we note that, thanks to the initial balanced condition of the MZI and to the integrated nature of this device, no thermal stabilization was needed to achieve a stable device operation. As a future perspective, we note that recent work [17] showed enhanced nonlinear optical performance of amorphous silicon waveguides, showing a higher γ parameter (about 3x that of c-Si) together with a higher TPA threshold (2x); thus suggesting the possibility of realizing an improved device able to achieve $\Delta\phi = \pi$, and hence a 100% power level switching of the probe signal.